POAC'15
Trondheim, Norway

Proceedings of the 23rd International Conference on
Port and Ocean Engineering under Arctic Conditions
June 14-18, 2015
Trondheim, Norway

CHARACTERISTICS OF UNDER-ICE OCEAN CURRENTS MEASURED DURING WAVE PROPAGATION EVENTS IN THE BARENTS SEA

A.V. Marchenko[1,2], V.V. Gorbatsky[3] and I.D. Turnbull[4]
[1]Arctic Technology Department, UNIS, N-9171 Longyearbyen, Norway
[2]Department of Civil and Transport Engineering, NTNU, N-7491 Trondheim,Norway
[3]Krylov State Research Center, 196158 St.-Petersburg, Russia
[4]Centre for Arctic Resource Development, NL Canada A1C 3X5, Canada

ABSTRACT
The propagation of surface waves in ice-covered waters can produce significant changes in the structure of floating ice over relatively short time periods and over very large open water areas. The effect is controlled by wave speeds and wave energy dissipation in ice conditions. Investigations of under-ice currents were performed during the expeditions by the RV Mikhail Somov (Russia) and the RV Lance (Norway). Turbulent characteristics of the currents were studied using data obtained from an Acoustic Doppler Velocimeter (ADV) SonTek Hydra 5MHz installed underneath the drifting ice in a downward-looking position. In 2014, the swell was also recorded using a Datawell buoy installed on the drifting ice. Despite a relatively long period of observations, only four events of wave propagation were registered and analyzed. In most of the events the dominant wave period was around 12 seconds. The influences of turbulent characteristics of under-ice currents and ice drift on the energy dissipation rates of waves propagating below continuous ice cover are investigated in the present paper.

INTRODUCTION
Propagation of surface waves below continuous floating ice is accompanied by new processes of the energy dissipation in comparison with surface waves propagating in water with an ice-free surface. The difference is explained by the influence of friction at the ice-water interface and of the ice viscosity on the energy dissipation. Friction at the ice-water interface influences the production of vorticity and turbulence in the boundary layer directly beneath the ice. A surface boundary layer also exists in open water, but in this case shear stresses are equal to zero at the water surface and energy dissipation rates are much smaller. Turbulence in the boundary layer below the ice is generated due to the relative movements of the water and ice which are driven by the ice drift, ocean currents, and wave penetration below the ice.
The influence of the eddy viscosity on the wave damping below a continuous ice cover was discussed by Liu and Mollo-Christinsen (1987). They derived the temporal decay and spatial rates of monochromatic plane waves propagating in water of infinite depth covered by an elastic ice sheet, and demonstrated that the results of the damping rate compare reasonably well with observations in the marginal ice zone (Wadhams, 1978; Weber, 1987). In the present paper we consider the results of field measurements of water velocities beneath a drifting ice floe during three events of wave propagation in the Barents Sea in April 2006 and 2012, and one event of wave propagation offshore Svalbard in the Store Fjord in April 2014. The collected data are used for the reconstruction of the eddy viscosity, turbulent

characteristics of the under-ice water boundary layer, and estimates of the wave damping below the ice.

METHOD FOR THE CALCULATION OF THE EDDY VISCOCITY

Turbulent shear stress applied to the ice at the ice-water interface is usually parameterized by the formula

$$\tau = -\rho K \frac{\partial \langle v_h \rangle}{\partial z}, \quad (1)$$

where ρ is the water density, $\langle v_h \rangle$ is the mean horizontal velocity of the water relative to the ice, z is the vertical coordinate, and K is the eddy viscosity. The mean horizontal velocity is calculated by averaging the relative water velocities over a time-scale much larger than a representative time-scale for turbulent fluctuations in the boundary layer. In our studies representative time-scales for turbulent fluctuations correspond to the sampling intervals of the measurements: 0.1-0.2s. The eddy viscosity depends on the flow processes in the boundary layer and is not as accurately determined as the molecular viscosity.

Turbulent shear stresses applied to the ice bottom could also be calculated as Reynolds stresses,

$$\tau_R = \rho \langle v_h' w' \rangle, \quad (2)$$

where v_h' and w' are the fluctuations of the horizontal and vertical velocities of the water below the ice.

The fluctuations velocities are determined as follows. When waves propagate below the ice the velocity vector field $\mathbf{v} = (u, v, w)$ of water particles can be represented as a sum,

$$\mathbf{v} = \langle \mathbf{v} \rangle + \mathbf{v}_w + \mathbf{v}', \quad (3)$$

where $\langle \mathbf{v} \rangle = \langle \mathbf{v}_h \rangle$ is the horizontal vector of the mean water velocity with absolute value $\langle v_h \rangle$, $\mathbf{v}_w$ is the water velocity induced by the waves, and $\mathbf{v}'$ is the fluctuation velocity. It is assumed that the mean velocity is changing slowly relative to the time-scale of the wave period, and the representative time-scale of the fluctuations is smaller than the wave period.

In-situ measurements of water velocities below the ice were performed by the Acoustic Doppler Velocimeter (ADV) SonTek Hydra 5MHz. The ADV was mounted in a downward-looking position on a tripod standing on the drifting ice floe. The ADV deployments used burst sampling. The burst sampling is specified by thee values: the sampling rate, the number of samples per burst, and the time between the start of successive bursts (called the burst interval).

Table 1. User setups of the ADV.

N	Data	Sampling frequency, Hz	Burst Interval, s	Samples per burst	Number of bursts	Depth, cm
1	April 24, 2006	5	1800	8000	2	190
2	April 25, 2006	10	1200	900	3	180
3	April 18-19, 2012	10	1200	1200	50	112
4	April 25, 2014	10	1200	3000	50	41

Collected data were processed to estimate the eddy viscosity and turbulent characteristics of the water flow in the under-ice boundary layer. The mean velocity is calculated by the formula,

$$\langle \mathbf{v} \rangle_\alpha = \frac{1}{N} \sum_{i=1}^{N} \mathbf{v}_i, \ \mathbf{v}_i = \mathbf{v}\big|_{t=t_\alpha + (i-1)\Delta T}, \quad (4)$$

where $\mathbf{v}_i$ is the value of the water velocity measured in the time $t = t_\alpha + (i\text{-}1)\Delta T$, ΔT is the sampling interval, N is the number of samples per burst, and time $t = t_\alpha$ specifies the start time of the burst α. Wave-induced velocities in the burst α were calculated with the Moving Average procedure as follows,

$$\mathbf{v}_{w,\alpha,j} = \mathbf{v}_w\big|_{t=t_{\alpha,j}} = \frac{1}{N_w}\sum_{i=j}^{j+N_w}\mathbf{v}_i\ ,\ \ t_{\alpha,j} = \frac{1}{N_w}\sum_{i=j}^{j+N_w}t_\alpha + (i-1)\Delta T\ , \tag{5}$$

where N_w is the number of samples over which the averaging is applied. The value of N_w is chosen to be much less than the number of samples in the wave period estimated by spectral analysis of the raw data. The velocities $\mathbf{v}_i$ and $\mathbf{v}_{w,\alpha,j}$ were interpolated over the interval $N\Delta T$ and performed in the form of a discrete time-series for each burst. Then the values of the fluctuation velocities $\mathbf{v}'$ were calculated from Equation (3) in the form of a discrete time-series of length N for each burst.

Components of Reynolds stresses applied to the ice were calculated using Equation (2) for the burst α,

$$\tau_{u,\alpha} = \frac{\rho}{N}\sum_{i=1}^{N}u'_{\alpha,i}\,w'_{\alpha,i}\ ,\ \ \tau_{v,\alpha} = \frac{\rho}{N}\sum_{i=1}^{N}v'_{\alpha,i}\,w'_{\alpha,i}\ . \tag{6}$$

The absolute value of the turbulent shear stress and vertical gradient of the mean horizontal velocity in the burst α were calculated with the formula,

$$\tau_\alpha = \sqrt{\tau_{u,\alpha}^2 + \tau_{v,\alpha}^2}\ ,\ \left|\partial\langle v_h\rangle_\alpha / \partial z\right| \approx \langle v_h\rangle_\alpha / h_\alpha\ , \tag{7}$$

where $\langle v_h\rangle_\alpha = \sqrt{\langle u\rangle_\alpha^2 + \langle v\rangle_\alpha^2}$ and h_α is the mean distance from the ice bottom to the point of the water velocity measurement in the burst α. The eddy viscosity in the burst α was estimated from Equations (1) and (2) with assumption that $\tau = \tau_R$ as follows,

$$K_\alpha = h_\alpha\tau_\alpha / (\rho\langle v_h\rangle_\alpha)\ . \tag{8}$$

The kinetic energies of waves ($\langle K_w\rangle_\alpha$) and their fluctuations ($\langle K_t\rangle_\alpha$) are given for the burst α by the formulas,

$$2\langle K_w\rangle_\alpha = \frac{1}{N}\sum_{i=1}^{N}\mathbf{v}_{w,\alpha,i}^2\ ,\ 2\langle K_t\rangle_\alpha = \frac{1}{N}\sum_{i=1}^{N}\mathbf{v}'^2_{\alpha,i}\ . \tag{9}$$

FIELD WORK LOCATIONS

In the present paper, we analyze data collected in four locations where field work was performed on the drifting ice and surface waves were measured underneath the ice. In 2006 the field work on the drifting ice in the Barents Sea was organized by the vessel Mikhail Somov within the Shtokman project of the laboratory Arctic-shelf (AARI). Surface waves propagating below the ice were registered by the ADV deployments 1 and 2 performed on April 24 and 25 on two floes 70km from one other in the Northwest direction. Figure 1a shows the region of this field work on the ice map. In 2012 and 2014 the field work on the drifting ice was organized by UNIS according to the study plan of the courses AT-208 (2012) and AT-211 (2014) and performed from the vessel RV Lance. In 2012 the RV Lance was moored to the drifting ice about 30km from Edgeoya (Fig. 1b). Surface waves propagating below the ice were registered by the ADV deployment 3 performed on April 18 and 19 on the same floe. In 2014 the RV Lance was moored to the drifting floe in Store Fjord (Fig. 1c). Surface waves propagating below the ice were registered by the ADV deployment 4 performed on April 25 and by the Datawell Directional Waverider DWR-G 0.4m buoy placed on the ice a few meters from the ADV during April 24-26.

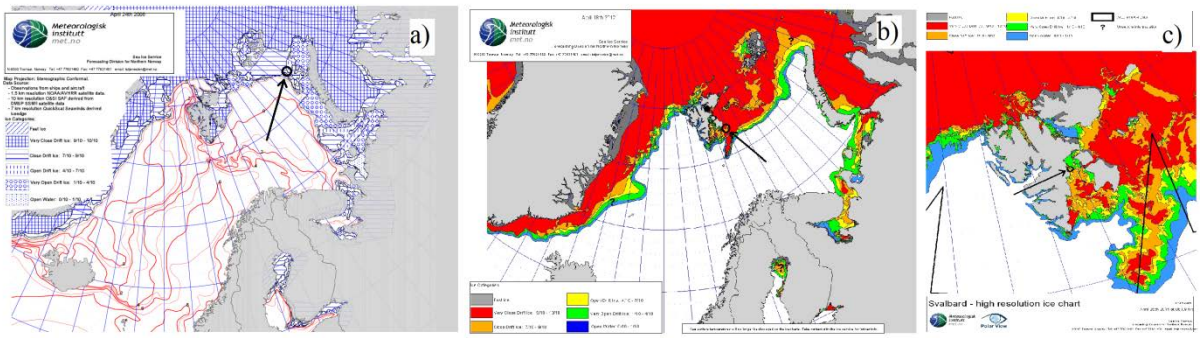

Figure 1. Locations of ADV deployments 1 and 2 (a), 3 (b) and 4 (c) are shown by arrows.

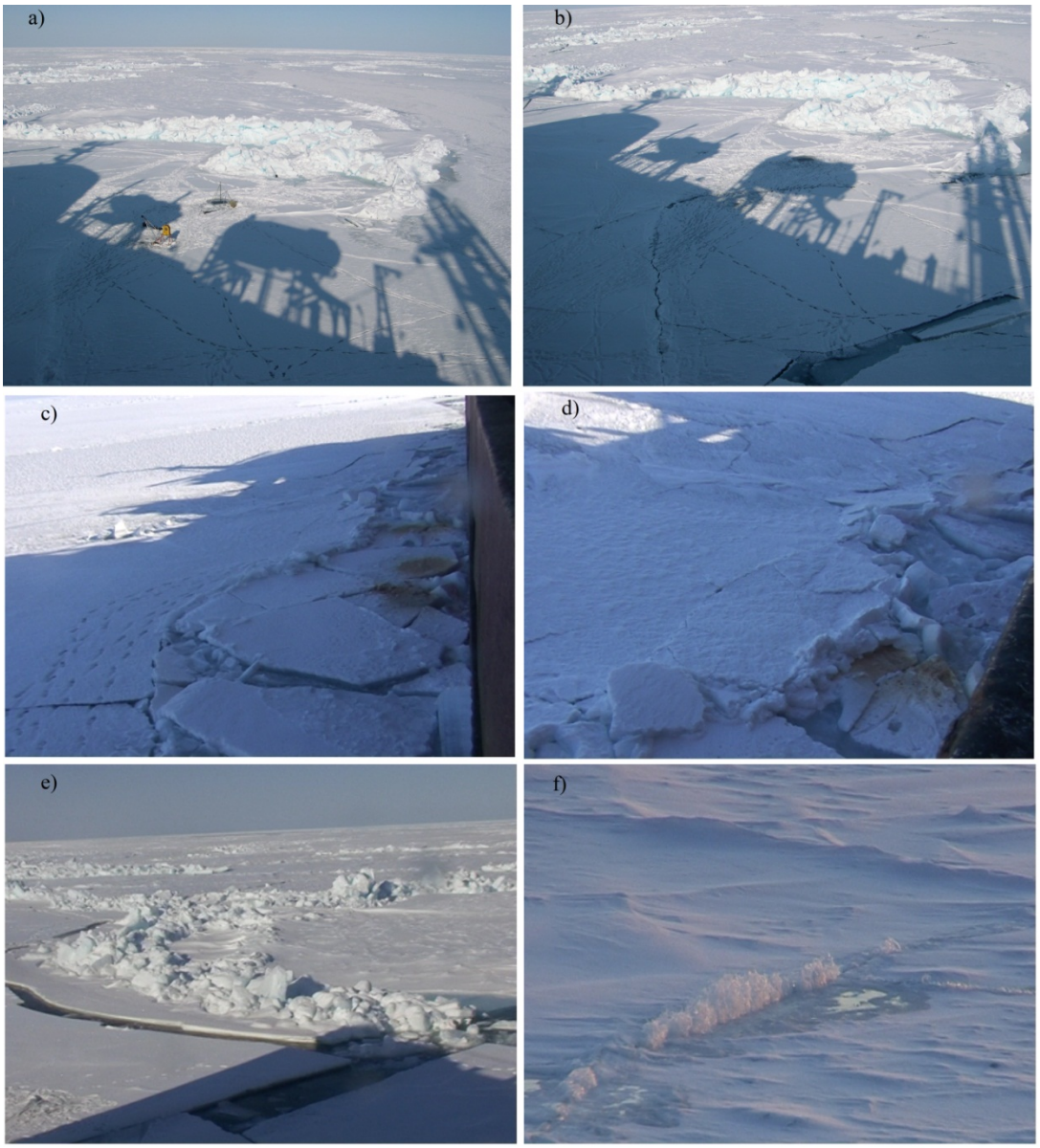

Figure 2. Location of the deployment 1 before (a) and after (b) the ice break-up by waves. Ice rafting near the ship board caused by the wave action (c, d). Divergence (s) and collisions (f) of floes caused by wave action.

Photographs of the locations of the deployments 1, 3 and 4 are shown in Fig. 2 and 3. The deployment 1 was performed between big ice ridges with sail heights up to 3m and the RV

Mikhail Somov (Fig. 2a). The surface of the surrounding ice cover was relatively flat. The deployment 2 was performed on the level ice. The deployment 3 was performed on the ice with multiple but not very large ridges with sail heights smaller than 2m (Fig. 3a). The deployment 4 was performed on the level ice floe (Fig. 3b). The thickness of level ice was about 60cm in the locations of all four ADV deployments.

The water depth was 200m in the deployment locations in 2006 and 2012, and 60m in the deployment location in 2014. Trajectories and velocities of ice drift were calculated using the vessel navigational data while they were moored to the ice floes (Figure 4). Figure 4a shows the trajectory of the RV Mikhail Somov from April 23, 16:15 GMT to April 24, 9:00 GMT, 2006. Figure 4b shows the trajectory of the RV Lance from April 18, 10:33 GMT to April 19, 23:59, GMT, 2012. Figure 4c shows the trajectory of the RV Lance from April 25, 00:00 GMT to April 25, 23:59, GMT, 2014. Figure 4b shows that the RV Lance followed the trajectory of the drifting ice with looping patterns caused by the combined actions of the semidiurnal tide and wind-induced inertial oscillations during the deployment 3. Drift trajectories in Figures 4a and 4c do not show looping patterns. The hodograph diagrams of the drift velocities are shown in Figure 5. They show that the drift speeds of the RV Lance during the deployment 3 reached 53cm/s, while the speeds of the RV Mikhail Somov moored to the drifting ice on April 23-24, 2006, and the RV Lance moored to ice on April 25, 2014, were less than 10cm/s and 15cm/s, respectively.

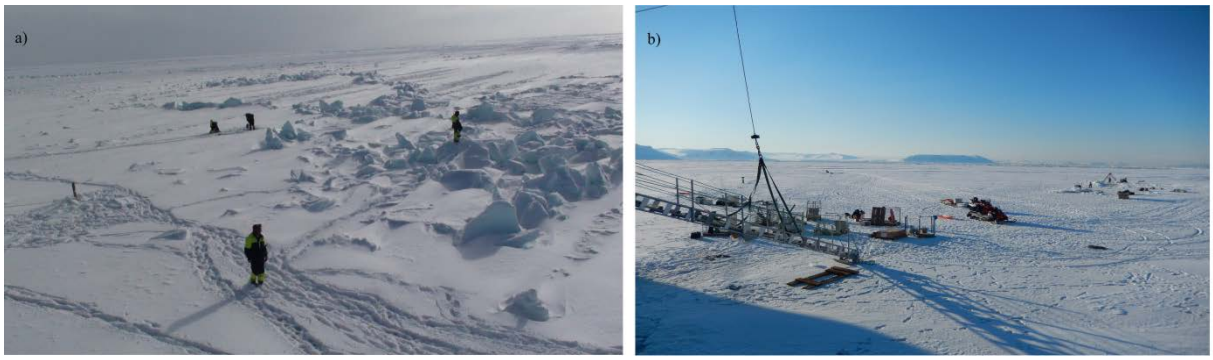

Figure 3. Deployment locations 3(a) and 4(b).

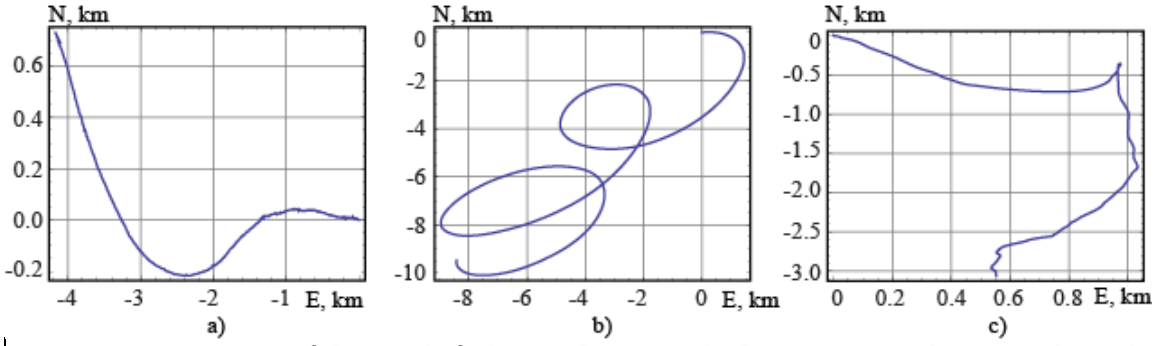

Figure 4. Trajectories of the ice drift during the ADV deployments 1 and 2 (a), 3 (b) and 4 (c).

The highest amplitude waves were registered in 2006 during the deployment 1 on April 24. The deployment 1 was aborted due to ice failure by wave action. Figures 2a and 2b show the ice around the deployment location 1 before and after the ice break-up by incoming waves. We also observed ice rafting near the ship board (Figures 2c-d), and dynamic divergence and collisions of floes (Figures 2e-f) around the ship caused by the wave action. Floe collisions were apparent from the vertical water jets produced by the contact interaction of floes (Figure 2f). We do not know when surface waves first appeared in the field work location. They were

recognized visually around 05:00 GMT, and the first cracks in the ice appeared around 08:00 GMT.

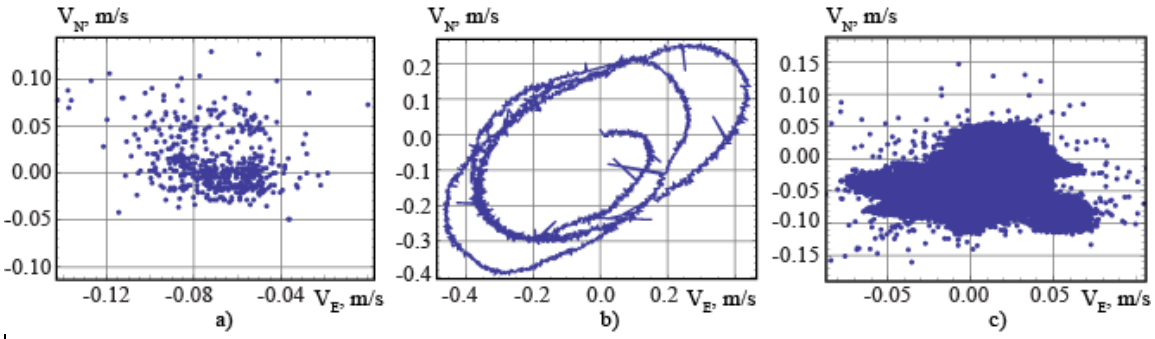

Figure 5. Hodograph diagrams of the ice drift velocities during the ADV deployments 1 and 2 (a), 3 (b) and 4 (c).

DATA ANALYSIS

User setups of the four ADV deployments are shown in Table 1. The depth column shows the depths of the ADV pressure sensors. Due to the location of the pressure sensor on the end cap of the ADV probe the actual depth of the velocity measurement is 55cm greater than the depths shown in Table 1. For the calculation of the mean distance h_α from the ice bottom to the point of the velocity measurements, the ice draft of about 55cm was subtracted from the actual depths of velocity measurements.

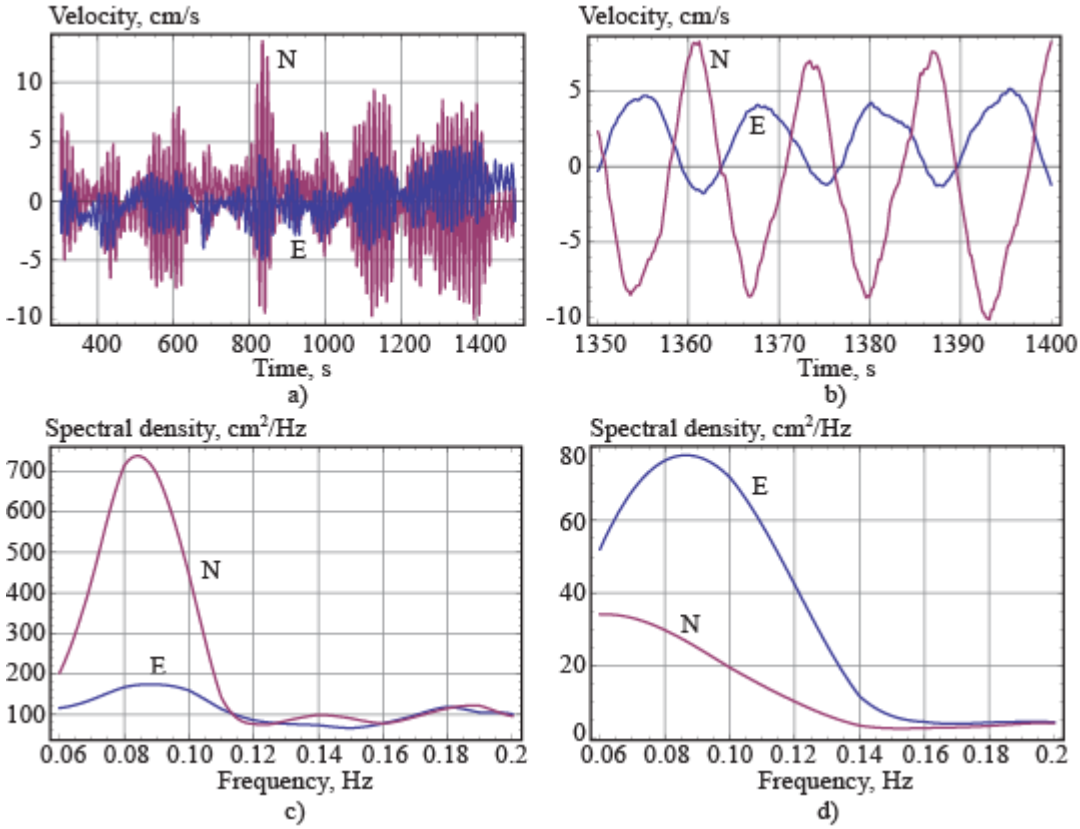

Figure 6. Records of zonal and meridional water velocity components in deployment 1 (a-b). Spectral densities in deployments 1 (c) and 2 (d).

Figure 6 shows fragments of ADV records during the deployment 1 over 23 minutes (a) and 50 seconds (b). Maximum amplitudes of horizontal water velocities below the ice reached

15cm/s. The wave period was about 12.5s. Figure 6b shows the water velocities versus the time when the ice was already partially broken up by waves. Figure 6a shows low-frequency wave modulations with periods varying from 100s to 200s. Graphs of the spectral densities calculated for the deployments 1 and 2 by SonTek ViewHydra Pro v2.93 software are shown in Fig. 6c and Fig. 6d, respectively. One can see that the direction of wave propagation has changed from the north-northwest to the north from the deployment 1 to the deployment 2, and wave amplitudes became much smaller during the deployment 2 in comparison with the deployment 1.

Figures 7a-b show fragments of ADV records during the deployments 3 and 4. Waves during the deployment 3 were very irregular but still recognized by the spectral analysis shown in Fig.7c. They propagate in the northerly direction and the amplitude of the meridional component of the water velocity oscillating with the frequency 0.1Hz is less than the amplitude of modulations with a period around 100s. Waves during the deployment 4 are more regular and better recognized in Fig.7b in comparison with Fig.7a, but the amplitudes of the water velocities shown in Fig.7b are even smaller than in Fig.7a. Spectral densities shown in Fig.7d show two frequencies 0.09Hz and 0.08Hz for the waves propagating in the meridional and zonal directions.

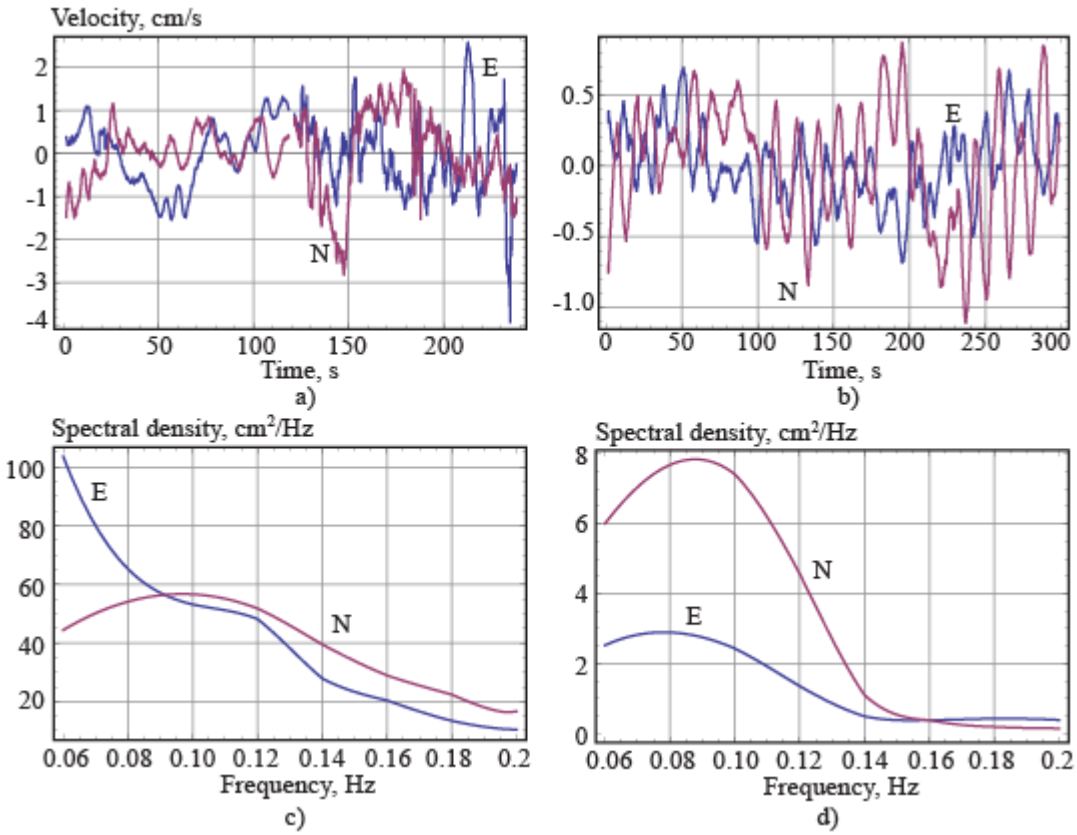

Figure 7. Records of meridional and zonal water velocity components in deployments 3(a) and 4(b). Spectral densities in deployments 3(c) and 4(d).

Figures 8a-b show the half-hourly mean vertical displacement of the ice floe and the zero-upcross frequency vs. the maximum spectral density, respectively, in deployment 4 (April 25-27) as registered by the Directional Waverider buoy deployed on top of the ice. For the April 25-27 period, the mean vertical heave response of the ice floe to the underlying surface waves was 0.03cm, with a maximum heave of 0.19cm occurring on April 25 (Fig. 8a). The maximum spectral densities of the ice floe response to wave action occurred at frequencies of around 0.05-0.06Hz and nearly 0.08Hz (Fig. 8b).

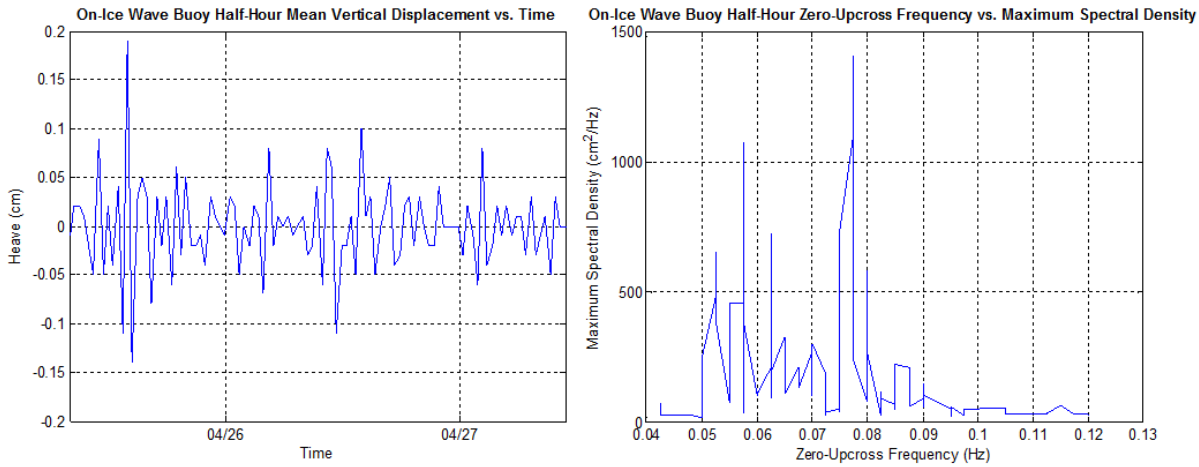

Figure 8. Records of half-hourly mean vertical displacement of the ice floe (a) and the zero-upcross frequency vs. the maximum spectral density (b) during deployment 4.

Table 2. Characteristics of under-ice boundary layer in deployments 1 and 2.

N	α	$\langle v_h \rangle$, cm/s	$\langle K_w \rangle$, cm^2/s^2	$\langle K_t \rangle$, cm^2/s^2	K, cm^2/s
1	1	2.96	5.14	0.44	0.23
	2	2.44	8.49	0.43	0.27
2	1	0.11	$4.4 \cdot 10^{-5}$	$1.3 \cdot 10^{-3}$	0.002
	2	0.12	$8.2 \cdot 10^{-5}$	$1.3 \cdot 10^{-3}$	0.003
	3	0.11	$12.3 \cdot 10^{-5}$	$1.4 \cdot 10^{-3}$	0.002

Table 3. Mean characteristics of under ice boundary layer in deployments 3 and 4.

N	$\langle v_h \rangle$, cm/s	$\langle K_w \rangle$, cm^2/s^2	$\langle K_t \rangle$, cm^2/s^2	K, cm^2/s
3	5.24	2.68	13.98	96.07
4	6.9	0.6	0.2	0.1

Calculated characteristics of the under-ice boundary layer are shown in Tables 2 and 3 and in Fig.9-11. A maximum wave energy of 105.9 cm^2/s^2 was registered during the deployment 1. Maximum values of the water velocity relative to the ice (12.6cm/s), the energy of fluctuations (52cm^2/s^2) and the eddy viscosity (409cm^2/s) were registered during the deployment 3. The eddy viscosities reconstructed from the data recorded during the deployments 1, 2 and 4 are of the order of 0.1cm^2/s, while the mean eddy viscosity measured during the deployment 3 was greater by 1000 times and reached almost 100cm^2/s. This effect could be associated with an influence of ice drift on the generation of turbulence in the under-ice boundary layer.

Characteristics of the under-ice boundary layer measured during the deployments 3 and 4 are compared in Fig.9-11a and Fig.9-11b. From Fig. 9a and Fig.10a it follows that the influences of the water flow speed relative to the ice $\langle v_h \rangle$ and wave energy $\langle K_w \rangle$ on the eddy viscosity $\langle K \rangle$ are not important when the energy of fluctuations $\langle K_t \rangle$ is high. Figures 9b and 10b show the increase of the eddy viscosity with the increase of $\langle v_h \rangle$ and $\langle K_w \rangle$ when the energy of fluctuations is low. Figure 11 demonstrates the increase of the eddy viscosity with the increase of the fluctuation energy.

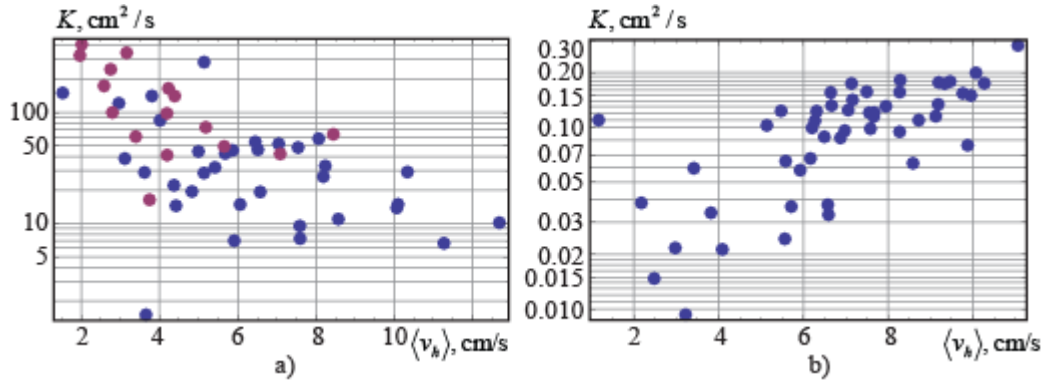

Figure 9. Eddy viscosity versus mean flow velocity in deployments 3 (a) and 4 (b).

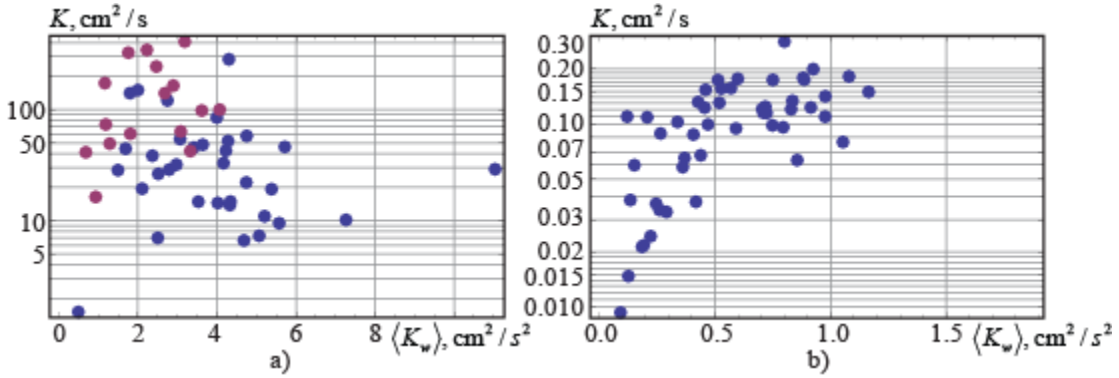

Figure 10. Eddy viscosity versus kinetic energy of waves in deployments 3 (a) and 4 (b).

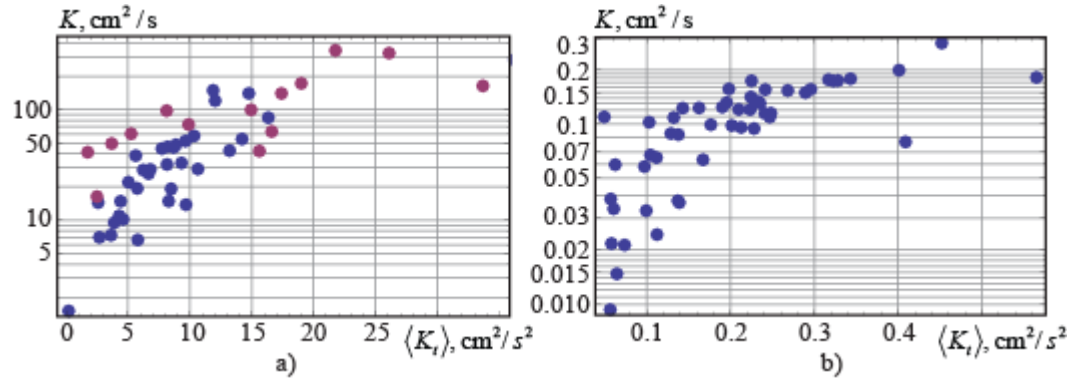

Figure 11. Eddy viscosity versus kinetic energy of fluctuations in deployments 3 (a) and 4 (b).

ESTIMATES OF WAVE DAMPING

The dispersion equation describing wave propagation in an ideal fluid covered by an elastic plate is given as follows (*e.g.*, Wadhams, 1973),

$$\omega^2 = k\tanh(kH)[g + Dk^4],\ D = Eh^3/[12\rho(1-\nu^2)], \tag{10}$$

where ω and k are the angular wave frequency and wave number, respectively, H is the water depth, and h, E and ν are the thickness, the effective elastic modulus and the Poisson's ratio of the ice, respectively. Representative values of E and ν are 2GPa and 0.33 (Marchenko et al., 2013), and the ice thickness is assumed to be 0.6m. The periods of observed waves were around 12s, and their angular frequency was $\omega \approx 0.52$rad/s. Simple calculations show that $k \approx 0.027\text{m}^{-1}$ when $\omega = 0.52$rad/s and $H = 200$m (deployment 1), and that $k \approx 0.029\text{m}^{-1}$ when $\omega = 0.52$rad/s and $H = 60$m (deployment 4). The wave lengths were about 232m during the

deployment 1 and 216m during the deployment 4. Further estimates show that $Dk^4 \approx 0.02\text{m}^2/\text{s}$ is much less than the gravitational acceleration $g = 9.81\text{m/s}^2$ in Equation (10). Therefore the influence of the ice elasticity can be neglected for the observed waves.

For the estimate of wave damping due to the friction on the ice-water interface we use the formula derived for the mean energy dissipation rate in oscillating water flow near a wall (formula (24.14) from Landau and Lifshitz, 1988),

$$\dot{\text{E}} = \frac{\rho k^2 \varphi_0^2}{2\sqrt{2}} \sqrt{\nu\omega}\,, \tag{11}$$

where φ_0 is the amplitude of the water velocity potential on the water surface, $k\varphi_0$ is the amplitude of the water velocity on the water surface, and ν is the kinematic viscosity. Wave energy is determined by the formula,

$$\text{E} = \frac{\rho\omega^2\eta_0^2}{2k\tanh(kH)}\,, \tag{12}$$

where $\eta_0 = k\varphi_0 \tanh(kH)$ is the wave amplitude. The attenuation rate of the wave amplitude due to the friction on the water surface is equal to,

$$\gamma_t = \frac{\dot{\text{E}}}{2\text{E}} = \frac{k\sqrt{\nu\omega}}{2\sqrt{2}\tanh(kH)}\,. \tag{13}$$

Equation (13) coincides with formula (A11) of Liu and Mollo-Christinsen (1988) derived for water with infinite depth when $\tanh(kH) = 1$. This approximation can be used when $k < 0.03\text{m}^{-1}$ and $H > 60\text{m}$. The temporal decay rate γ_t can be converted to a spatial decay rate γ_x by the formula (Caster, 1962),

$$\gamma_x c_g = \gamma_t\,,\ c_g = \partial\omega/\partial k\,. \tag{14}$$

The spatial decay rate divided by the wave number versus the kinematic viscosity is shown in Fig. 12. Two graphs are calculated for two values of the wave number $k \approx 0.027\text{m}^{-1}$ and $k \approx 0.029\text{m}^{-1}$ calculated from the dispersion Equation 10 with the same wave frequency $\omega \approx 0.52\text{rad/s}$ but with different water depths $H = 200\text{m}$ and $H = 60\text{m}$. One can see that $\gamma_x/k<1$ in both cases for the range of the kinematic viscosities coinciding with the range of the eddy viscosities reconstructed from the collected data. Simple estimates show that $\gamma_x \approx 1/(14\text{km})$ when $\nu = 100\text{cm}^2/\text{s}$.

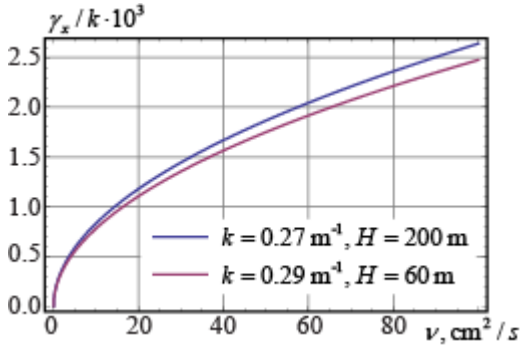

Figure 12. Spatial decay rate versus the kinematic viscosity.

CONCLUSIONS

Ice drift is most important for the generation of the turbulence in the under-ice boundary layer of the water. Kinetic energy of the turbulence fluctuations in the under-ice boundary layer influences the eddy viscosity and the decay rate of surface waves penetrating below the ice. The mean eddy viscosity estimated for the under-ice boundary layer near Edgeoya reaches $100cm^2/s$ with a maximum value of $409cm^2/s$. It influences the spatial decay of swells with a period of 12s over a distance of 14km.

REFERENCES

Caster, M., 1962. A note on the relation between temporally-increasing and spatially-increasing disturbances in hydrodynamic instability. J. Fluid Mech., 14, 222-224.

Landau, L.D., Lifshitz,E.M., 1988. Fluid Mechanics, Second edition: Vol. 6 (Course of Theoretical Physics S), Butterworth-Heinemann, Oxford.

Liu, A. K. and E. Mollo-Christensen (1988), Wave propagation in a solid ice pack, J. Phys. Oceanogr., 18(11), 1702-1712.

Marchenko, A., Kvamstad, B., Fjørtoft, K., Hoyland, K., Brazhnikov, D., 2011. Characteristics of ice drift in the Western Barents Sea reconstructed by the data of the trackers deployed on drifting ice in 2008 and 2010. POAC11-147, Montreal, Canada, 16 pp.

Wadhams, P., 1973. Attenuation of swell by sea ice. J. Geoph. Res., 78, 3552-3563.

Weber, J.E., 1987. Wave attenuation and wave drift in the marginal ice zone. J. Phys. Oceanogr., 17, 2351-2361.